INDIAN JOURNAL OF SCIENCE AND TECHNOLOGY

RESEARCH ARTICLE

Morphological Insights of Lithium-Phosphate Nano Compounds by Data Driven Pore Analysis of SEM Images with ML Algorithms

Sahith Battula[1,2], Nived Alla[1], Madipelli Sri Sai Pavan[1], Linganaboina Srinivasa Rao[3]*, B Chennakesava Rao[1]

1 Department of Mechanical Engineering, VNR Vignana Jyothi Institute of Engineering and Technology, Bachupally, Nizampet (S.O), Hyderabad, 500090, Telangana, India
2 Ruhr-University Bochum, Bochum, 44801, Germany
3 Centre for Nanoscience and Technology, Department of Physics, VNR Vignana Jyothi Institute of Engineering and Technology, Bachupally, Nizampet (S.O), Hyderabad, 500090, Telangana, India

OPEN ACCESS

Received: 08-08-2024
Accepted: 08-05-2025
Published: 30-05-2025

Editor: Special Issue Editors: Dr. N. Pothanna, Dr.T. Jayashree, Dr. V. Ganesh Kumar

Citation: Battula S, Alla N, Pavan MSS, Rao LS, Rao BC (2025) Morphological Insights of Lithium-Phosphate Nano Compounds by Data Driven Pore Analysis of SEM Images with ML Algorithms. Indian Journal of Science and Technology 18(SP1): 72-80. https://doi.org/10.17485/IJST/v18si1.icamada50

* **Corresponding author**.

srinivasarao_l@vnrvjiet.in

Funding: None

Competing Interests: None

Published By Indian Society for Education and Environment (iSee)

ISSN
Print: 0974-6846
Electronic: 0974-5645

Abstract

Objectives: To study how compositional changes (specifically, varying ZnO/Sb_2O_3 ratios) affect the pore properties of lithium-phosphate-copper nanocompounds, interpreting their morphographs by Machine Learning (ML) algorithms. **Methods:** Inorganic lithium-phosphate nanocompounds doped with copper (Cu) nanoparticles were synthesized by solid state reaction. The composition of the nanocompounds was modified by varying concentrations of modifiers namely, antimony oxide (Sb_2O_3) and zinc oxide (ZnO). The morphographs of the samples were recorded by Scanning Electron Microscope (SEM). In this paper, we have described a novel approach to pore detection in SEM images that employs ML algorithms. **Findings:** The proposed methodology was used to detect pores, calculate their length and area, and count total number of pores in the samples automatically. Furthermore, data visualization plots were drawn to show the distribution of pore lengths and the frequency of pores. According to the study, as ZnO content rises, average pore size increases from 0.939 μm^2 to 5.003 μm^2, while pore count significantly decreases from 471 to 153. **Novelty:** The data visualization allowed us to draw conclusions about the size distribution, density, and spatial arrangement of pores. The number of pores, total area of the pores, and fraction of area occupied by the pores found to be changed as a function of composition of the samples. Overall, this paper has provided a strong framework for automated pore analysis in SEM images of the prepared samples by ML algorithms.

Keywords: Nano Compounds; SEM Morpho Graphs; Pore Characteristics; Data Visualization; Machine Learning

1 Introduction

The multidisciplinary study of materials science and engineering is primarily concerned with investigating the physical, chemical, mechanical, thermal, electrical, magnetic, electronic, and optical properties of various solids[1,2]. Understanding porosity (shape and quantity of tiny gaps or pores) of a solid material and hence its aforementioned properties is very important for research and development in the fields of solid state sciences, building materials, electronics, and energy storage devices[3,4]. The porosity of materials can be advantageous or unfavorable depending on the type of application. Pores in a material can act as stress concentrators and reduce its mechanical strength and toughness. On the other hand, regulated porosity is frequently preferred in particular applications like energy storage, catalysis, and filtration due to increase in the surface area to volume ratio of the solids containing more number of pores. In order to understand and forecast the performance of engineering materials, the pore characteristics (such as number, size, shape, and distribution) must be investigated first. For the purpose of pore analysis, traditional techniques like mercury intrusion porosimetry and gas adsorption are available[5,6]. But, these techniques have several limitations as follows: i) they damage the samples, ii) they consume more time, and iii) they can only capture the spatial distribution of pores partially. To overcome such limitations, recently materials researchers have been acquiring high resolution surface images of materials and their cross-sections by means of advanced imaging techniques. In order to understand the surface morphology of solid materials, three important microscopic tools are available such as Scanning Electron Microscopy (SEM), Transmission Electron Microscopy (TEM), and Atomic Force Microscopy (AFM). Among these three imaging tools, SEM is a fundamental and inexpensive tool suitable for porous media[7].

SEM imaging is a prevailing tool in the areas of materials science & engineering, mining, and geology owing to its vast prospective to offer exclusive intuition into micro and nanoscale pores, scratches, defects, voids, etc. Asif Ali et al.[8] have reviewed characterization of various minerals with the help of SEM. This review has discussed the idea of assimilating robotics with SEM to design portable tools for mineral characterization not only on Earth, but also on other terrestrial planets. SEM imaging offers pore interpretation, which is a non-destructive and aesthetically pleasant approach, enabling direct observation and quantification of pore features[8].Manual interpretation of SEM pictures can be subjective, time-consuming, and prone to human error, especially when working with big datasets or intricate pore patterns. Due to this constraint, automated image analysis methods have been investigated, which use machine learning (ML) algorithms to speed up the pore identification and characterization process[9]. Machine Learning (ML) has become a supplementary quantitative microscopic software tool, combing with SEM for investigating the morphological features of the materials. Hee-Beom Lee & his group have reported the reliable porosity measurement of high capacitance- nickel oxide based cathode materials for developing Li- ion batteries using Deep Learning (DL) image segmentation[9]. In order to automate and expedite the process of pore identification and characterization, one complete strategy that combines the high-resolution imaging capabilities of SEM with the aid of ML algorithms is desperately needed. ML algorithms can overcome the drawbacks of manual analysis and obtain a deeper understanding of the complex relationship between pore characteristics and properties of material, which will ultimately lead to more intelligent material design and optimization strategies for practical applications[7–9].

Lithium-phosphate nano compounds are studied for energy storage, with SEM imaging used to analyze morphology like porosity and surface area. However, gaps remain in automating pore analysis, understanding the complex microstructure-performance relationships, and integrating machine learning (ML) with experimental work. Current methods are time-consuming, prone to error, and lack standardization, hindering cross-study comparisons. To address these issues, advanced ML models for automated image analysis, integration of multiple characterization techniques, real-time synthesis optimization, and a standardized image processing framework are needed. These improvements will enable more efficient design of high-performance nano compounds for energy storage[10,11]. Present research work aims to develop a scientific procedure, which comprises both the ML algorithms and SEM imaging techniques for a better understanding of surface morphology and porosity of the nano compounds. Therefore, we can measure the quantity, size, and distribution of pores by examining SEM pictures of the prepared nano compounds with different compositions[12]. This study addresses the gap by proposing a methodological framework that combines ML algorithms with SEM imaging, data visualization and statistical analysis to gain a deeper insight into the surface morphology and porosity of lithium-phosphate-copper nano compounds. This method may be instrumental in relating the pore characteristics in terms of the compositional change for optimizing the specific properties of nano compounds for practical applications.

2 Methodology

Four inorganic nano compounds doped with copper nanopowder (≈30 nm) were prepared by solid state reaction with a specific composition of $10Li_2O$-(30-x)Sb_2O_3-xZnO-59.5P_2O_5:0.5Cu (in mol %) as described in our earlier work[13]. Let us label these samples as LSZPC nano compounds. SEM morpho graphs of four samples, namely LSZPC-1, LSZPC-2, LSZPC-3, and LSZPC-

4 (at x = 0, 10, 20, and 30 mol % respectively) were captured by Oxford Aztec instruments. Novel approaches to extracting useful information from SEM images and data have been made possible by recent developments in ML, especially in the area of computer vision. Recently, software developers have been designing accurate and reliable models that can precisely identify and measure pores by preparing algorithms on labeled SEM images[14]. The porosity of the samples was automatically identified using a ML based method. The workflow of the methodology is shown in Figure 1.

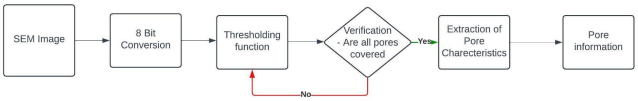

Fig 1. The flowchart to detect porosity of the samples

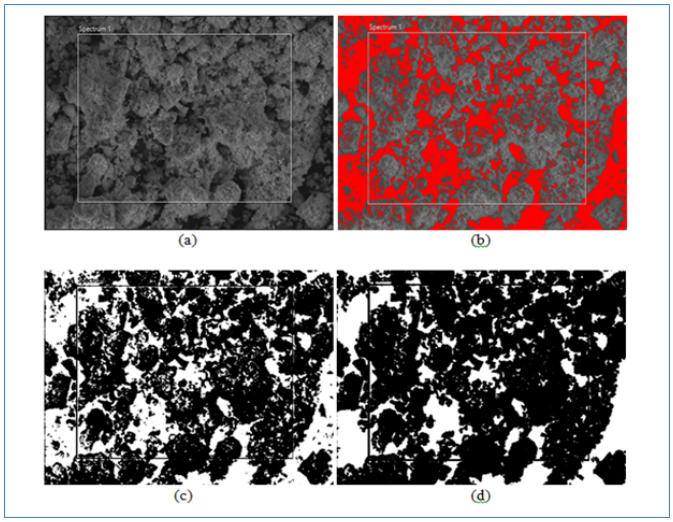

Fig 2. An illustration of porosity determination by SEM image with ML algorithm in lithium-phosphate nanocompounds; (a) Processed SEM image of the sample at x = 0 mol %, (b) Image segmentation by global thresholding method, (c) Binary form of the image with pores shown as black regions and the scaffold material as white regions, and (d) ML morphological processed SEM image including erosion and dilation

Using image processing techniques, the machine learning system was able to precisely determine the sizes and distributions of individual pores by segmenting the SEM images into pore and non-porous areas[15,16]. Here, we have illustrated the entire methodology for one of the samples (at x = 0 mol %). The pixel size units of SEM image (Figure 2 (a)) of the first sample (at x = 0 mol %) were converted to metric units (micrometers, μm) as the initial step in the machine learning software. To get the final pore size data on a single scale that was independent of the imaging magnification or scale factor, this conversion was required. The conversion procedure was carried out using the Image-J software[17]. To get the pixel-to-micrometer ratio, a line was drawn across the scale bar in the SEM picture and the scale bar's known distance (for example, 100 μm) was entered. Because it distinguished between the material and pore regions in the SEM images, image segmentation was an essential stage in the machine learning program. A global thresholding method based on histogram analysis was automatically used. Using this method, the picture histogram showed two separate peaks, which stood for the pores (dark parts) and scaffold material (bright parts) as shown in Figure 2 (b). The image was then divided into binary form, with pores shown as black regions and the scaffold material as white regions as shown in Figure 2 (c), using the algorithm, which first determined the lowest intensity value between these two peaks and utilized it as the threshold[15,16]. Because the pores in the SEM images were linked (or in contact) with one another, measuring their separate diameters was sometimes difficult. To solve this issue, the machine learning program made use of many morphological processes, including erosion and dilation; the final results of applying these processes is shown in Figure 2 (d). These techniques allowed the individual pore lengths to be measured by severing the connected pores. Increasing scaffold material regions could effectively reduce the pore spaces with dilation and break connections at the smallest joining points. The pixels filled with scaffold material are destroyed by the process of erosion, restoring the pore spaces to

the original values. Automated thresholding, binary conversion, and morphological filtering techniques allowed the machine learning system to accurately analyze the sizes and distributions of individual pores. The proposed method, therefore, accurately segments and separates regions of pores in SEM images [15,16].

3 Results and Discussion

Elhadidy et al. [18] have introduced threshold and watershed algorithms for segmentation of pore areas on the surface ultrafiltration membrane. They have developed the algorithms on AFM and SEM images of scaffolds and assessed the data against manually defined pores. This pore identification method is found to be rapid. It provides reproducible and reliable pore size distributions of the membrane. The average pore count (N) and average pore diameter of the membrane were identified as $50/\mu m^2$ and 8 nm respectively. Nilly Hojat et al. [19]have developed an image processing algorithm for automatic measurement of the pore sizes from the SEM images of porous scaffolds. Analysis of SEM images with the possible incorporation of ML algorithms is used to automate the procedure for identification and quantification of pores in the materials. This algorithm is used to provide automatic detection and precise determination of pore sizes and their distribution, showing consistent outcome of pore size in the range of 0.5-30 μm^2 with error ≈1.36 % as compared with respect to their actual size. In the previous studies, only the profiles of pore size and pore distributions have been evaluated [18,19]. But, in the present study, the ML software has produced comprehensive quantitative data on the various pore properties of the prepared LSZPC nano compounds as a function of variation of the composition [12]. The following pore parameters are assessed and presented in Table 1:

Table 1. Pore characteristics of LSZPC nano compounds obtained from SEM images with ML

Sample	Pore count (N)	Total area (A) μm^2	% Area (Porosity) (P)	Average size (S) μm^2	Circularity (C)	Solidity (S′)
LSZPC-1	471	1183.279	19.247	8.457	0.720	0.803
LSZPC-2	399	374.744	23.452	0.939	0.681	0.763
LSZPC-3	364	307.359	23.656	0.844	0.722	0.722
LSZPC-4	153	765.426	14.839	5.003	0.692	0.838

a) Pore count (N): For a given sample, this value indicates the total number of individual pores found and counted inside the SEM picture.

b) Total area (A): Within the studied region of SEM image, the total area parameter represents the entire area occupied by all of the pores. Typically, this value is expressed in μm^2.

c) Average size: The mean area of each individual pore found in the sample is provided by the average size parameter. The average pore size in square micrometers is obtained by dividing the total area by the count.

d) % Area or Porosity (P): The percentage area, also known as porosity, shows the portion of the entire examined area that is made up of pores. Porosity is the percentage of the pores area to the total focused area of the sample. Understanding this value is essential to determining the sample's total porosity and how it could affect characteristics like surface area, permeability, and mechanical strength.

e) Circularity (C): The degree to which the pore shapes approximate complete circles is indicated by the circularity metric. A perfect circle is indicated by a circularity value of 1.0, while increasing departure from a circular form is shown by values decreasing from 1.0. This measure sheds light on the irregularities and shape of the pores.

f) Solidity (S′): Solidity refers to the degree of how the volume of a material is packed with solid substances, which is the ratio of the solid area to the total volume of the sample.

3.1 Effect of compositional changes on pore characteristics

The systematic variation in the contents of zinc oxide (ZnO) and antimony trioxide (Sb_2O_3) in the composition considerably changed the observed pore characteristics. The first sample LSZPC-1 (at x = 0 mol % of ZnO) has the highest concentration of Sb_2O_3 (30 mol %). It has a relatively high pore count (N≈471), but a low average pore size (S≈8.457 μm^2) and total pore area (A≈1183.279 μm^2). The majority of the pores in this sample have reasonably good values of circularity (C≈0.720) and solidity (S′≈0.803), suggesting a more uniform and regular pore morphology [20]. The second sample LSZPC-2 (at x = 10 mol% of ZnO and 20 mol% of Sb_2O_3) has less Sb_2O_3 than in the first sample LSZPC-1, which showed decreased area (A≈374.744 μm^2) and total average size (S≈0.939 μm^2) of the pores. These variations of the pore properties might be due to the presence of ZnO in the sample composition, which might further affect the sintering mechanism and kinetics in pore generation [21]. Coming to the third sample LSZPC-3, the content of Sb_2O_3 has gone down to 10 mol% and the content of ZnO is 20 mol% in this sample.

The count of pores further drops down to N≈364. Overall pore area (A≈307.359 μm^2) and the average pore size (S≈0.844 μm^2) are much less in this sample compared to the second sample LSZPC-2. The ZnO based nanocomposites having lowest values of pore size, which suggests that they can exhibit high capacitance and such materials may find applications as electrodes in supercapacitors and energy storage devices[22]. Fourth sample LSZPC-4 does not contain any Sb_2O_3, and it contains the highest ZnO content (30 mol %). The number of pores in this sample is the lowest as N≈153. At the same time, the average size of the pores (S≈5.003 μm^2) and total pore area (A≈14.839 μm^2) are higher than that of the third sample LSZPC-3. The fourth sample LSZPC-4 has exhibited lower circularity (C≈0.692) and solidity (S′≈0.692) values of the pores, depicting the higher complexity and irregularity in pore morphology. Doping of ZnO up to 30 mol % in the composition has shown the highest solidity and the lowest porosity of the sample LSZPC-4. The pore size and pore distribution could be influenced by the presence of high content of ZnO in the LSZPC samples[23].

The LSZPC samples have uniform, circular, and solid morphologies of the pores with rich content of Sb_2O_3.As the concentration of ZnO increases up to 30 mol % in the composition, the LSZPC samples have been gradually transformed into irregular, complex, diversified pore structures. This observation shows that compositional modification plays an essential role in the microstructural development during the synthesis process by solid state reaction. These results will establish how elementary oxides, such as ZnO (refractory oxide) can influence viscosity, phase separation, and grain boundary dynamics of the materials[24], whereas Sb_2O_3 (semi glass former) can have tendency of grain growth and pore development nature of nanocompounds[25]. The derived pore compositions and pore formation mechanisms can be instrumental in understanding complex pore morphologies in terms of ratio of ZnO/Sb_2O_3 in the composition. Sb_2O_3 is a well-known glass former and could be responsible for increasing the viscous flow and forming amorphous phases during sintering[16]. This statement is further supported by the presence of increased amounts of the more regular and circular-shaped pore architectures in samples LSZPC-1 and LSZPC-2. On the other hand, ZnO is a refractory oxide (with a higher melting point than Sb_2O_3) and does display an underlining, but noticeable sintering tendency[23]. Based on this concept, one can work on the development of rational strategies for designing of nanoc ompounds that can simultaneously optimize the interplay of composition with the pore characteristics and allow optimization of the porous materials for the various applications such as building materials, energy storage, tissue engineering, catalysis, etc[3,4,9,12,22]. Therefore, present study may offer a tool for designing new high-performance porous materials.

3.2 Visualization of pore characteristics across samples

Table 1 shows the interrelation between compositional variables and pore characteristics for LSZPC nanocompound samples. The pore count is observed to decrease from LSZPC-1 to LSZPC-4. The above results indicate that high Sb_2O_3-rich compositions seem to support pore formation. More interestingly, the total pore area of the samples as a function of composition is nonlinear. LSZPC-1 shows the highest value of pore area (A≈1183.279 μm^2). This anomaly in LSZPC-1 is further reflected in its larger average pore size (S≈8.457 μm^2), indicating that high Sb_2O_3 content increases not only pore count but also allows the formation of larger pores[26].

Quite interestingly, the porosity in percentage area does not follow a linear trend with composition. The porosity (P) peaks for LSZPC-2 and LSZPC-3 at 23.452% and 23.656% respectively. This observation suggests optimal compositional ratio of Sb_2O_3/ZnO is needed for obtaining the maximum extent of the porosity (P). The values of circularity remain almost constant in all samples and exhibit a slightly small decrease in LSZPC-2. Solidity creates a U-shaped trend with more significant values at the extremes of composition, namely LSZPC-1 and LSZPC-4, pointing out that high content of Sb_2O_3 and high ZnO equally support more solid and less fragmented pore structures[20,23].

Figure 3 represents a comprehensive box plot view of the distribution of pore characteristics for the LSZPC nano compound samples. This plot shows the variability and central tendencies for some of the main morphological parameters. In Figure 3 , the red line represents the median of each dataset. In a general box plot the box itself represents the interquartile range, which include the middle portion of the dataset, and the whiskers extend to the minimum and maximum values within a range. The red line shows the 50^{th} percentile which is the median.

The most striking features are the high dispersions of Total area (in μm^2), expressed by the large extension of the box and whiskers from 300 to 1200 μm^2. That wide range underscores how large effect compositional variations have on total pore area (A). The next largest spread exists in the pore count (N), which has a median of about 400 pores, ranging from 150 to 470, thus putting a strong effect of composition in underlining the pore formation dynamics. The % area (Porosity) is relatively narrowly distributed, indicating that despite variations in other variables, the net porosity (P) remains more or less the same for all samples considered in this study, having a median of about 20%. The distribution of average size (S)is highly skewed, with the lower quartile somewhat compact and the upper whisker stretching far off, thus indicating that most samples have comparatively smaller average pore sizes, but there is a potential for far larger pores under some compositional conditions. The most restricted

distributions are seen in circularity (C) and solidity (S′), suggesting that these shape-related properties are relatively invariant to compositional changes[27]. In contrast to the size and count variability, this stability in pore shape metrics is sharp, which points out that although composition has a strong influence on pore formation and growth, it does not much affect their geometry. These observations lead to important insights into the complex interplay of the nano compound composition and their resultant pore morphologies, evidencing areas of high sensitivity and robustness in the structural characteristics of the material[27].

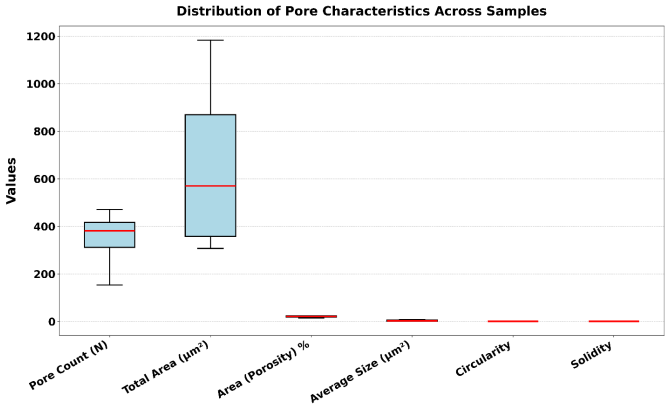

Fig 3. Box plot for the distribution of pore characteristics across samples

Furthermore, a set of scatter plots have shown the correlations between the ZnO content and several pore properties in the LSZPC nano compounds are shown in Figure 4. These graphs show the intricate, frequently nonlinear interactions between pore morphology and composition[24]. The important outcomes are as follows:

i) An increase in ZnO content is strongly correlated negatively with pore count (N). The trend line indicates that pore development is strongly inhibited by increasing concentration of ZnO, since there is a sharp fall from roughly 500 holes at 0 mol % of ZnO to about 200 pores at 30 mol% of ZnO.

ii) ZnO content shows a non-linear relationship with total area (A). Between 0 and 10 mol% ZnO, there is a steep decline; and at higher concentrations, there is a small increase. This non-monotonic behavior suggests that composition and total pore area (A) are intricately entwined.

iii) The porosity percentage area (P) exhibits a mild parabolic trend that peaks at moderate concentration of ZnO (about 10–20 mol %). This implies that there is a range of compositions that are best for optimizing porosity, with lower total porosity occurring at both high and low concentration of ZnO.

iv) The ZnO content shows a U-shaped relationship with average size (A). At both low (0 mol %) and high (30 mol %) of ZnO, larger holes are seen, while smaller pores are seen at intermediate levels. This suggests that at each end of the composition spectrum, extreme compositions encourage the creation of bigger pores.

v) Although the association is weak, circularity (C) exhibits a minor negative tendency as ZnO content increases. The little change (about 0.72 to 0.69) indicates that the concentration of ZnO has very little effect on the regularity of pore morphology.

vi) ZnO content shows a weak positive connection with solidity (S′). Over the ZnO range, the trend line exhibits a modest increase from roughly 0.77 to 0.80, suggesting that slightly more solid, less fragmented pore architectures may result from higher ZnO concentrations.

The majority of plots, particularly the total area (A) and average size (S) have large confidence intervals or shaded areas. Significant uncertainty is shown in these relationships, which may be due to a small number of data points or other contributing factors not taken into consideration in this method. The studies with more data points across the composition range may provide refinement of these trends in the future[28]. These discoveries not only advance our knowledge of the structure-composition interactions in LSZPC nano compounds but also lay the groundwork for the thoughtful design of materials with specialized porosities for a variety of practical applications.

Aleksandra Głowska et al. have investigated spatial heterogeneity of γ-Alumina, combining SEM image analysis with deep learning, the study not only improves our ability to quantify pore structures but also provides predictive insights into how these structures affect mass transfer and, consequently, catalytic performance[29]. Deep-learning-based method, using the Pore-net model, for the intelligent identification and quantitative characterization of pores in shale SEM images has been studied by Chen et al[30]. This method offers valuable insights for evaluating shale oil and gas reservoirs and studying other porous materials. However, these models show reduced accuracy when characterizing porous media, especially nano compounds. The porosity

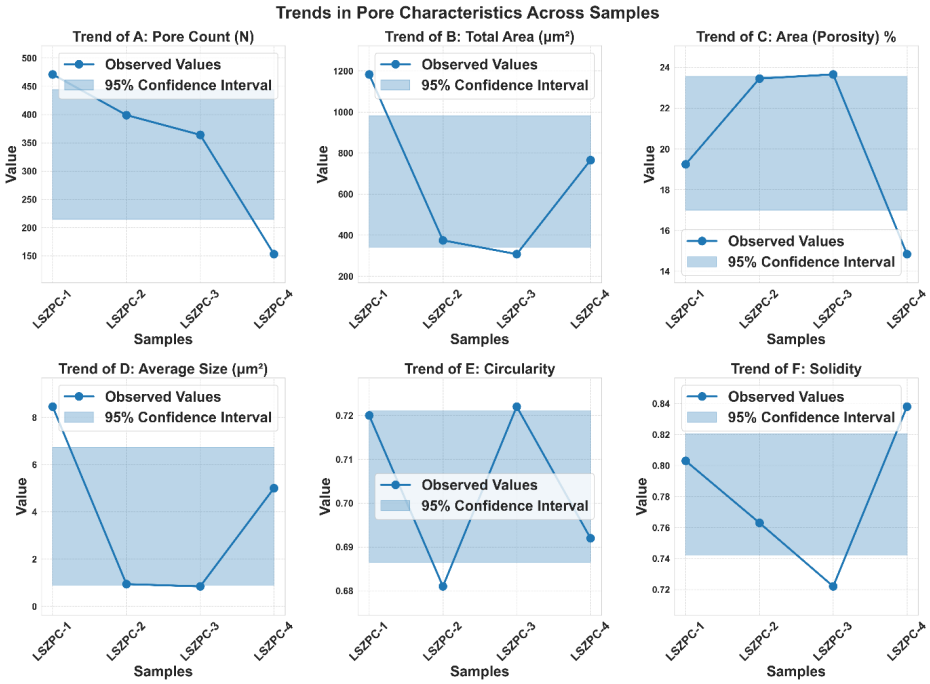

Fig 4. Scatter plots of the trends observed in the pore characteristics of the samples

calculations often exhibit significant deviations from experimental data. On the other hand, the advantage of the present model is its ability to automate and accurately quantify pore features of nano compounds such as porosity, particle size, and surface area, using machine learning algorithms, thereby enhancing the efficiency and precision of morphological analysis compared to traditional (manual) methods. This approach enables faster, scalable, and more reliable correlation between microstructure and electrochemical performance, improving material design for energy storage applications.

4 Conclusion

SEM morphographs of Cu nanoparticles doped- lithium phosphate nano compounds modified by varying content of Sb_2O_3/ZnO were recorded. A novel ML approach to pore detection in SEM images of the samples was proposed, which could act as an alternative method to manual methods with high efficiency and good reliability. From the ML analysis of SEM images, the number of pores was observed in the range of 153 - 471 in the samples, whereas the fractional area occupied by the pores was identified as 14% - 23% of the total surface area of the samples. The pore count is highest in the sample LSZPC-1 and it is lowest in LSZPC-4. The higher values of circularity and solidity have been observed for the samples LSZPC-2 and LSZPC-3, which were composed of both modifiers - Sb_2O_3 and ZnO. Thus, the compositional dependence of morphological parameters has been investigated by ML algorithms. Unlike traditional manual methods that are time-consuming and prone to human error, this ML-based method provides a high-efficiency, reliable, and alternative procedure for studying the pore characteristics. The integration of machine learning into SEM image analysis holds significant promise for future research and industrial applications. The ability to efficiently analyze pore distribution and characteristics could facilitate the development of more optimized nanocompounds with tailored properties for specific applications. For instance, the precise understanding of pore morphology can lead to advancements in materials used in catalysis, energy storage, and filtration systems. ML-based approach by combining SEM data with X-ray diffraction or spectroscopy results could provide a more comprehensive understanding of the material properties.

5 Acknowledgement

The authors thank the management of **VNRVJIET**, Hyderabad for supporting this work. This paper has been presented in "International Conference on Applied Mathematics and Advanced Data Analytics for Industry 5.0 (ICAMADA-2024)" held from 25th to 27th April 2024 at VNR VJIET, in collaboration with APTSMS and CCOE. The authors express their

sincere gratitude to the guest editors for their tireless efforts and dedication by means of comments, editing and overseeing the manuscripts to bring to this final form.

The APC is deferred partially by the Indian Society for Education and Environment.

References

1) Rahimi-Ahar Z, Ahar LR. Thermal, optical, mechanical, dielectric, and electrical properties of nanocomposites. *European Polymer Journal*. 2024;218. Available from: https://doi.org/10.1016/j.eurpolymj.2024.113337.
2) Rao LS, Hussain S, Navalika A, Rao BC, Rao TV, Hila FC. Effect of ZnO nanoparticles on physical, optical and radiation shielding properties of Bi2O3-B2O3-Cr2O3 glasses. *Results in Optics*. 2023;12. Available from: https://dx.doi.org/10.1016/j.rio.2023.100491.
3) Sarna-Boś K, Skic K, Sobieszczański J, Boguta P, Chałas R. Contemporary Approach to the Porosity of Dental Materials and Methods of Its Measurement. *International Journal of Molecular Sciences*. 2021;22(16). Available from: https://pmc.ncbi.nlm.nih.gov/articles/PMC8396236/.
4) Al-Maharma AY, Patil SP, Markert B. Effects of porosity on the mechanical properties of additively manufactured components: a critical review. *Materials Research Express*. 2020;7(12). Available from: https://dx.doi.org/10.1088/2053-1591/abcc5d.
5) Guo J, Zhang X, Lu C, Chai Z, Kang G, Zhao G, et al. Characterization of Pore Structures with Mercury Intrusion Porosimetry after Electrochemical Modification: A Case Study of Jincheng Anthracite. *ACS Omega*. 2022;7(13):11148–11157. Available from: https://dx.doi.org/10.1021/acsomega.1c07286.
6) Medina-Rodriguez BX, Alvarado V. Use of Gas Adsorption and Inversion Methods for Shale Pore Structure Characterization. *Energies*. 2021;14(10). Available from: https://doi.org/10.3390/en14102880.
7) Alqaheem Y, Alomair AA. Microscopy and Spectroscopy Techniques for Characterization of Polymeric Membranes. *Membranes*. 2020;10(2). Available from: https://dx.doi.org/10.3390/membranes10020033.
8) Ali A, Zhang N, Santos RM. Mineral Characterization Using Scanning Electron Microscopy (SEM): A Review of the Fundamentals, Advancements, and Research Directions. *Applied Sciences*. 2023;13(23). Available from: https://dx.doi.org/10.3390/app132312600.
9) Lee HB, Jung MH, Kim YH, Park EB, Jang WS, Kim SJ, et al. Deep learning image segmentation for the reliable porosity measurement of high-capacity Ni-based oxide cathode secondary particles. *Journal of Analytical Science and Technology*. 2023;14. Available from: https://dx.doi.org/10.1186/s40543-023-00407-z.
10) Gabbett C, Doolan L, Synnatschke K, Gambini L, Coleman E, Kelly AG, et al. Quantitative analysis of printed nanostructured networks using high-resolution 3D FIB-SEM nanotomography. *Nature Communications*. 2024;15(1). Available from: https://www.nature.com/articles/s41467-023-44450-1.
11) Chen X, Tang X, Xiong J, He R, Wang B. Pore characterization was achieved based on the improved U-net deep learning network model and scanning electron microscope images. *Petroleum Science and Technology*. 2025;43(7):715–729. Available from: https://doi.org/10.1080/10916466.2024.2326178.
12) Muda MM, Legese AM, Urgessa G, Boja T. Strength, Porosity and Permeability Properties of Porous Concrete Made from Recycled Concrete Aggregates. *Construction Materials*. 2023;3(1):81–92. Available from: https://dx.doi.org/10.3390/constrmater3010006.
13) Rao LS, Rao BC, Battula S, Alla N. Morphology, physical, and structural aspects of copper nanoparticles induced- metal phosphate nanocompounds for gamma ray shielding and magnetic sensing applications. *Inorganic Chemistry Communications*. 2024;166. Available from: https://dx.doi.org/10.1016/j.inoche.2024.112588.
14) Wang H, Xu F, Cai L, Salvato D, Lemma FGD, Capriotti L, et al. A fine pore-preserved deep neural network for porosity analytics of a high burnup U-10Zr metallic fuel. *Scientific Reports*. 2023;13(1). Available from: https://dx.doi.org/10.1038/s41598-023-48800-3.
15) Thilagashanthi T, Gunasekaran K, Satyanarayanan KS. Microstructural pore analysis using SEM and ImageJ on the absorption of treated coconut shell aggregate. *Journal of Cleaner Production*. 2021;324. Available from: https://dx.doi.org/10.1016/j.jclepro.2021.129217.
16) Cole ME, Stout SD, Dominguez VM, Agnew AM. Pore Extractor 2D: An ImageJ toolkit for quantifying cortical pore morphometry on histological bone images, with application to intraskeletal and regional patterning. *American Journal of Biological Anthropology*. 2022;179(3):365–385. Available from: https://doi.org/10.1002/ajpa.24618.
17) Schroeder AB, Dobson ETA, Rueden CT, Tomancak P, Jug F, Eliceiri KW. The ImageJ ecosystem: Open-source software for image visualization, processing, and analysis. *Protein Science*. 2021;30(1):234–249. Available from: https://pmc.ncbi.nlm.nih.gov/articles/PMC7737784/.
18) ElHadidy AM, Peldszus S, Van Dyke MI. Development of a pore construction data analysis technique for investigating pore size distribution of ultrafiltration membranes by atomic force microscopy. *Journal of Membrane Science*. 2013;429:373–383. Available from: https://dx.doi.org/10.1016/j.memsci.2012.11.054.
19) Hojat N, Gentile P, Ferreira AM, Šiller L. Automatic pore size measurements from scanning electron microscopy images of porous scaffolds. *Journal of Porous Materials*. 2023;30(1):93–101. Available from: https://dx.doi.org/10.1007/s10934-022-01309-y.
20) Reddy NR, Kumar AS, Reddy PM, Kakarla RR, Jung JH, Aminabhavi TM, et al. Efficient synthesis of 3D ZnO nanostructures on ITO surfaces for enhanced photoelectrochemical water splitting. *Journal of Environmental Management*. 2024;352. Available from: https://dx.doi.org/10.1016/j.jenvman.2024.120082.
21) Borges OH, Cardoso ALF, Moreira MH, Klein-Gunnewiek RF, Pandolfelli VC. Conventional and microwave-assisted sintering of ZnO-containing CAC-bonded alumina-based refractory castables. *Journal of the European Ceramic Society*. 2023;43(14):6562–6570. Available from: https://dx.doi.org/10.1016/j.jeurceramsoc.2023.06.063.
22) Ates M, Alperen C, Bayrak Y, Yoruk O. Pore size, conductivity and surface area effects of rGO/ZnO/PTh hybrid nanocomposite for supercapacitors. *Diamond and Related Materials*. 2024;147. Available from: https://dx.doi.org/10.1016/j.diamond.2024.111230.
23) Reda AE. Effect of ZnO on sintering and microwave dielectric properties of 0.5CaTiO3-0.5 (Li0.5La0.5) TiO3 ceramics. *Journal of the Indian Chemical Society*. 2023;100(2). Available from: https://doi.org/10.1016/j.jics.2023.100901.
24) il Kim S, An J, Lee WJ, Kwon S, Nam W, Du N, et al. Effect of ZnO and SnO2 Nanolayers at Grain Boundaries on Thermoelectric Properties of Polycrystalline Skutterudites. *Nanomaterials*. 2020;10(11). Available from: https://dx.doi.org/10.3390/nano10112270.
25) Wang R, Zhou T, Zhong Z. Low-temperature processing of LiZn-based ferrite ceramics by co-doping of V2O5 and Sb2O3: Composition, microstructure and magnetic properties. *Journal of Materials Science & Technology*. 2022;99:1–8. Available from: https://dx.doi.org/10.1016/j.jmst.2021.06.003.
26) Shaikh ZA, Raut SD, Danamah HM, Kamble C, Shinde PV, Shaikh SF, et al. Solution-processed Sb2O3: A promising electrode material for high-performance supercapacitors and electrocatalysts. *Journal of Energy Storage*. 2024;89. Available from: https://dx.doi.org/10.1016/j.est.2024.111736.
27) Hejduk A, Czajka S, Lulek J. Impact of co-processed excipient particles solidity and circularity on critical quality attributes of orodispersible minitablets. *Powder Technology*. 2021;387:494–508. Available from: https://dx.doi.org/10.1016/j.powtec.2021.03.063.

28) Ito C, Maeda T, Higashi R, Osada T, Kohata T, Ozaki S. Application of extreme value statistics to internal pore distribution in ceramics and prediction of size dependency of strength scatter. *Journal of the European Ceramic Society*. 2024;44(5):3381–3392. Available from: https://dx.doi.org/10.1016/j.jeurceramsoc.2023.12.021.
29) Głowska A, Jolimaitre E, Hammoumi A, Moreaud M, Sorbier L, de Faria Barros C, et al. SEM Image Processing Assisted by Deep Learning to Quantify Mesoporous γ-Alumina Spatial Heterogeneity and Its Predicted Impact on Mass Transfer. *The Journal of Physical Chemistry C*. 2024;128(20):8395–8407. Available from: https://dx.doi.org/10.1021/acs.jpcc.4c00323.
30) Tang X, He R, Wang B, Zhou Y, Yin H. Intelligent Identification and Quantitative Characterization of Pores in Shale SEM Images Based on Pore-Net Deep-Learning Network Model. *Petrophysics – The SPWLA Journal of Formation Evaluation and Reservoir Description*. 2024;65(2):233–245. Available from: https://dx.doi.org/10.2139/ssrn.4525391.